

Memristor Model Comparison

Alon Ascoli, Fernando Corinto, Vanessa Senger, and Ronald Tetzlaff

Abstract

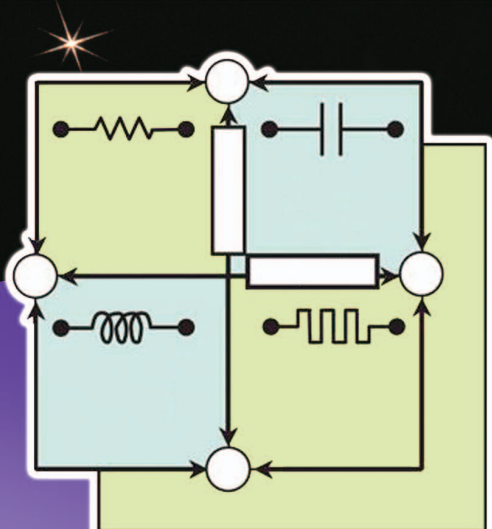
Since the 2008-dated discovery of memristor behavior at the nano-scale, Hewlett Packard is credited for, a large deal of efforts have been spent in the research community to derive a suitable model able to capture the nonlinear dynamics of the nano-scale structures. Despite a considerable number of models of different complexity have been proposed in the literature, there is an ongoing debate over which model should be universally adopted for the investigation of the unique opportunities memristors may offer in integrated circuit design. In order to shed some light into this passionate discussion, this paper compares some of the most noteworthy memristor models present in the literature.

The strength of the Pickett's model stands in its experiment-based development and in its ability to describe some physical mechanism at the origin of memristor dynamics. Since its parameter values depend on the excitation of the memristor and/or on the circuit employing the memristor, it may be assumed as a reference for comparison only in those scenarios for which its parameters were reported in the literature. In this work various noteworthy memristor models are fitted to the Pickett's model under one of such scenarios. This study shows how three models, Biodek's model, the Boundary Condition Memristor model and the ThrEshold Adaptive Memristor model, outperform the others in the replica of the dynamics observed in the Pickett's model. In the second part of this work the models are used in a couple of basic circuits to study the variance between the dynamical behaviors they give rise to. This analysis intends to make the circuit designers aware of the different behaviors which may occur in memristor-based circuits according to the memristor model under use.

I. Introduction

The memristor was theoretically envisioned by Prof. Chua back in 1971 [1]. This device is characterized by a nonlinear relation between

Memristors: Theory and Applications



charge and flux, i.e. the time integrals of current and voltage. It follows that the resistance of the memristor depends on the time history of the current flowed through it or of the voltage fallen across it in case of charge or flux control respectively. The memristor exhibits a set of unique fingerprints ([2], [3]) among which a current-voltage pinched hysteretic loop under periodic excitation. However, as shown in [4], the current-voltage representation does not uniquely defines a memristor. It is the charge-flux relation which does it instead [5].

A few years after the 1971 proposal the memristor was classified as the simplest element within a larger class of dynamical systems, namely the memristive systems [6]. Despite it was recently proved [7] that a classical purely-passive electronic circuit made up of a nonlinearly-resistive two-port cascaded with a linear dynamic one-port acts as a volatile memristive system, non-volatile memristive behavior may not be observed in any circuit employing already available circuit components [5]. However, an exciting discovery, which took place at Hewlett Packard (HP) Labs [8] in 2008, proved the

Due to the model dependency of the nonlinear dynamics occurring in memristor-based circuits, there is an urgent need for the development of an ultimate mathematical model for the physical nano-device to foster progress in memristor-based IC design.

existence of non-volatile memristive behavior in nature, specifically in a Titanium dioxide-based nano-film. Since then, the industry has been engaged in the search for novel materials and technologies for the manufacture of these nano-structures [9]. In parallel, a considerable amount of work has been devoted to the development of mathematical models capable to reproduce the complex dynamics exhibited by these nano-devices. The availability of accurate, general and simple models is crucial for the investigation of the nonlinear dynamics of memristor-based circuits ([10], [11]), to develop novel hybrid [12] hardware architectures combining memory storage and data processing in the same physical location and at the same time [13], and to explain the memristive behavior of biological systems ([14], [15]).

To the best of the authors' knowledge, the real value of Pickett's model [16] lies in the fact that it was derived on the basis of experiments. Furthermore, it gives some hint on the physical mechanisms at the origin of the unique behavior of the TiO_2 -based memristor nano-film. In this work the Pickett model is simulated using the PSpice implementation presented in [17].

In the first part of this paper, under a particular triangular excitation for which the Pickett model parameter values were reported in [17], a number of models of memristor nano-structures reported in the literature (Joglekar's [18], Bielek's [19], Prodromakis' [20], the Boundary Condition Memristor (BCM) model [22] and the ThrEshold Adaptive Memristor (TEAM) model [23]) are fitted to the Pickett model through an optimization procedure based upon a combination of Simulated Annealing [24] and Gradient Descent [25] algorithms.

In the second part of this manuscript the various models are then used in a couple of basic circuits to study the variance of the dynamical behaviors they give rise to. A final discussion on the comparison between the models raises awareness of the model-dependency of the dynamics of memristor-based circuits. As a result, the design of novel memristor-based architectures requires the preliminary determination of a universal memristor model. In the next years industry and academia should join their forces to address this crucial issue.

Finally we give some hint on a novel kind of charge-controlled memristor model in which the state equation governing the time evolution of the state may be expressed as a series of polynomials involving state and input current. Preliminary studies reveal that a modeling approach based upon power series representation of the state evolution function [6] has the potential to exhibit desirable features such as flexibility, accuracy and simplicity.

The manuscript is structured as it follows. Section II gives a brief overview of the Pickett model and of the models under comparison. Section III presents the optimization procedure and specifies the parameters of the optimized models under a well-documented scenario. Section IV describes simulations of memristor-based circuits employing various memristor models and discusses the variance between the observed behaviors. Section V comments on advantages and disadvantages of the models. Section VI introduces a novel memristor modeling approach. Finally Section VII outlines conclusions and future research developments.

II. Memristor Models

This section first introduces the reference model and then the models under comparison. For the sake of brevity the explicit time-dependency of variables is dropped.

A. Reference Model

The reference model is Pickett's model [16], which explains the mechanisms at the origin of the complex dynamics observed in the TiO_2 -based memristor by means of the Simmons tunnel barrier model [26]. A PSpice implementation of the Pickett model, presented in [17], shall be used in this manuscript to run simulations on the reference model. The other models, described in Section II-B, shall be simulated in Matlab. According to the Pickett model, after an electroforming process, in a certain central region of the TiO_2 -based memristor most of the film sandwiched between the Platinum electrodes, except for a narrow tunnel barrier of length w (defined as the system state), is shunted

Alon Ascoli, Vanessa Senger, and Ronald Tetzlaff are with the Faculty of Electrical and Computer Engineering, Technische Universität Dresden, Dresden, Germany. Fernando Corinto is with the Department of Electronics and Telecommunications, Politecnico di Torino, Torino, Italy. E-mails: alon.ascoli@mailbox.tu-dresden.de, vanessa.senger@tu-dresden.de, ronald.tetzlaff@tudresden.de, and fernando.corinto@polito.it. The authors equally contributed to the manuscript.

by an oxide layer enriched with oxygen vacancies (a TiO_{2-x} -based highly conductive channel) whose resistance is named R_s . When a current i flows through the nano-device, naming v the voltage across the whole memristor, the voltage falling across the tunnel barrier, let us call it v_g , is given by $v_g = v - R_s i$. The equation governing the time evolution of the state variable w is

$$\frac{dw}{dt} = f_{\text{off}} \sinh\left(\frac{|i|}{i_{\text{off}}}\right) \exp\left(-\exp\left(\frac{w - a_{\text{off}}}{w_c} - \frac{|i|}{b}\right) - \frac{w}{w_c}\right) \quad (1)$$

for $i > 0$, while it is

$$\frac{dw}{dt} = -f_{\text{on}} \sinh\left(\frac{|i|}{i_{\text{on}}}\right) \exp\left(-\exp\left(\frac{a_{\text{on}} - w}{w_c} - \frac{|i|}{b}\right) - \frac{w}{w_c}\right) \quad (2)$$

for $i < 0$. In the optimization procedure of Section III we shall refer to the memristor-circuit of Fig. 1, where the input voltage source v_i is a periodic triangular signal, represented in Fig. 2 over one period, and has a series resistance $R_i = 2.4 \text{ k}\Omega$. In [17] the memristor dynamics in this circuit were experimentally described and modeled. Under this scenario the mean values of the parameters in (1)–(2), as reported in [17], are tabulated in Table 1. Furthermore, R_s was set to 215Ω .

The current through the device is modeled as a tunneling junction current [26]:

$$i = \frac{j_o A}{(\Delta w)^2} \{ \phi_I e^{-B\sqrt{\phi_I}} - (\phi_I + e|v_g|) e^{-B\sqrt{\phi_I + e|v_g|}} \}, \quad (3)$$

where $A = 10^4 \text{ nm}^2$ is the average channel area of the memristor and j_o and λ are expressed by

$$j_o = \frac{e}{2\pi h}, \lambda = \frac{L_m}{w},$$

where $e = 1.6 \cdot 10^{-19} \text{ C}$ is the elementary electronic charge, $h = 6.6 \cdot 10^{-34} \text{ Js}$ is the Planck constant, $k = 5$ is the mean value of the dielectric constant, $\epsilon_o = 8.854 \cdot 10^{-12} \text{ F m}^{-1}$ is the vacuum permittivity and $L_m = e^2 \ln(2) / 8\pi\kappa\epsilon_o$ is expressed in eV m . Furthermore, in equation (3) w_1 and w_2 are defined as

$$w_1 = \frac{1.2\lambda w}{\phi_o}, w_2 = w_1 + w \left(1 - \frac{9.2\lambda}{3\phi_o + 4\lambda - 2e|v_g|} \right),$$

where $\phi_o = 0.95 \text{ eV}$ is the mean value of the barrier height, while the expressions for B and ϕ_I are

$$B = \frac{4\pi\Delta w\sqrt{2m}}{h}$$

$$\phi_I = \phi_o - e|v_g| \frac{w_1 + w_2 - 1.15\lambda w}{\Delta w} \ln\left(\frac{w_2(w-w_1)}{w_1(w-w_2)}\right),$$

where $\Delta w = w_2 - w_1$ and $m = 9.1 \cdot 10^{-31} \text{ kg}$ is the electron mass.

B. Models Under Comparison

Let us introduce the models under comparison, i.e. Joglekar's model [18], Bielek's model [19], Prodromakis' model [20], the BCM model [22] and the TEAM model [23].

In all these models except the last one, the memristor is modeled as a thin oxide film of length D comprising a conductive layer of oxygen-deficient Titanium dioxide TiO_{2-x} with length w (chosen as the state variable)

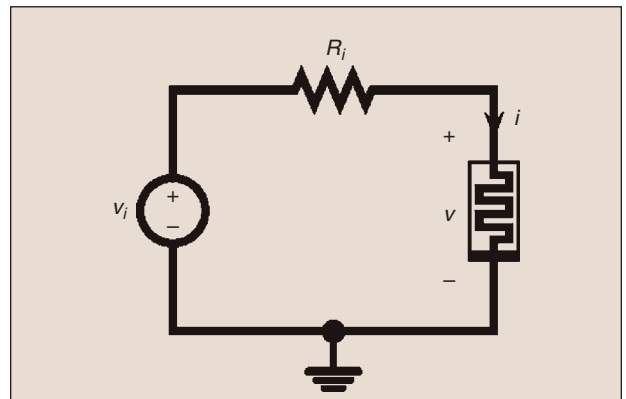


Figure 1. Memristor-based circuit used in the optimization strategy of Section III.

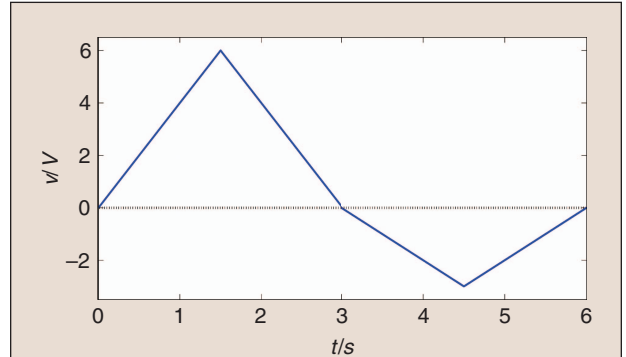


Figure 2. Triangular excitation of the circuit of Fig. 1. Only one period is shown.

Table 1.
Values of the parameters in the state equations (1)–(2) of the reference model under triangular excitation of the circuit of Fig. 1.

f_{off}	f_{on}	i_{off}	i_{on}
$3.5 \mu\text{ms}^{-1}$	$40 \mu\text{ms}^{-1}$	$115 \mu\text{A}$	$8.9 \mu\text{A}$
a_{off}	a_{on}	b	w_c
1.2 nm	1.8 nm	$500 \mu\text{A}$	107 pm

In the original linear oxygen vacancy drift model proposed by Williams, the input is in current form, and the model is valid only for certain choices of input and initial state.

serially connected with an insulating layer of stoichiometric Titanium dioxide TiO_2 of length $D - w$.

In such models the memristor input u -output y relation may be modeled as

$$y = M\left(\frac{w}{D}\right)u \quad (4)$$

for current-control, i.e. $u = i$ and $y = v$, where $M(\cdot)$ denotes the memristance function defined as

$$M\left(\frac{w}{D}\right) = R_{\text{off}} - \Delta R \frac{w}{D}, \quad (5)$$

where R_{on} and R_{off} are the memristor resistances when the whole nano-film is respectively enriched and depleted with oxygen vacancies and $\Delta R = R_{\text{off}} - R_{\text{on}}$. For voltage control, i.e. $u = v$ and $y = i$, the input u - output y relation becomes

$$y = W\left(\frac{w}{D}\right)u, \quad (6)$$

where $W(\cdot)$ represents the memductance function expressed by

$$W\left(\frac{w}{D}\right) = \frac{G_{\text{on}}G_{\text{off}}}{G_{\text{on}} - \Delta G \frac{w}{D}}, \quad (7)$$

where $G_{\text{on}} = R_{\text{on}}^{-1}$, $G_{\text{off}} = R_{\text{off}}^{-1}$ and $\Delta G = G_{\text{on}} - G_{\text{off}}$.

The equation governing the time evolution of the state is

$$\frac{dw}{dt} = \mu \frac{R_{\text{on}}}{D} i f(w, u), \quad (8)$$

where μ denotes the average mobility of the oxygen vacancies, while $f(w, u)$ is a window function which may take into account boundary behavior and various nonlinear dynamical effects such as nonlinear oxygen vacancy drift. In the optimization procedure outlined in Section III the initial values of the parameters in equations (4) (for $u = i$) or (6) for $u = v$ and (8) are set to $R_{\text{on}} = 1 k\Omega$, $R_{\text{off}} = 10 k\Omega$, $\mu = 10^{-16} m^2 V^{-1} s^{-1}$ and $D = 10 \text{ nm}$, while the initial state is chosen as $w(0) = 2.2222 \text{ nm}$.

In the original linear oxygen vacancy drift model proposed by Williams [8] the input is in current form (i.e. $u = i$) and $f(w, i) = 1$ for all w and for all i . This model is valid only for those choices of input and initial state which guarantee the state w to assume values in $[0, D]$.

Let us give the mathematical expression for the window function in models [18]–[22]. In Joglekar's model [18], where $u = i$, $f(w, i) \in [0, 1]$ is independent of the current and may assume its maximum unitary value at $w = 0.5 D$ according to

$$f(w, i) = f(w) = 1 - \left(\frac{2w}{D} - 1\right)^{2p}, \quad (9)$$

where p is a positive integer controlling the rate of decrease of the state variable as it approaches either bound (the optimization procedure of Section III shall sweep this parameter). In case w assumes one of its two bounds, it shall never leave it thereafter, irrespective of the input. This is in contradiction with what occurs in practice.

In order to circumvent such issue, keeping the input in current form, Biolek [19] introduced a novel window function $f(w, i) \in [0, 1]$, which, through the introduction of discontinuous transitions occurring under any sign reversal in the input, may switch from its minimum null value to its maximum unitary value at either bound. The expression of this window is the following:

$$f(w, i) = 1 - \left[\frac{w}{D} - \text{stp}(-i)\right]^{2p}, \quad (10)$$

where p is a positive integer controlling the rate of decrease of the state variable from each bound to the other one (a sweep of this parameter shall be considered in the optimization procedure of Section III), and $\text{stp}(i)$ is defined as

$$\text{stp}(i) = \begin{cases} 1 & \text{if } i \geq 0, \\ 0 & \text{if } i < 0. \end{cases}$$

In Prodromakis' model [20] $u = i$ and the window function $f(w, i)$, independent of i , is described by

$$f(w, i) = f(w) = j \left\{ 1 - \left[\left(\frac{w}{D} - 0.5 \right)^2 + 0.75 \right]^p \right\}, \quad (11)$$

where $p \in \mathbb{R}_+$ and $j \in \mathbb{R}_+$ are two controlling parameters which co-determine both the rate of decrease of the window function as the state variable approaches any of its two bounds and the maximum value of the window function itself, which may here exceed the unitary value (the optimization process outlined in Section III sweeps both p and j).

As analytically demonstrated in [22], under sign-varying control voltage source Joglekar's and the

Biolek's models may only capture single-valued and multi-valued memductance-flux characteristics respectively. The BCM model, offering the opportunity to tune the boundary behavior and the non-volatility degree according to the dynamics under modeling, does not suffer from this limitation, since through proper tuning both single-valuedness and multi-valuedness may arise on the memductance-flux plane under the mentioned excitation. In this model the input is assumed in voltage form, i.e. $u = v$, and the window function is expressed as

$$f(w, v) = \begin{cases} b & \text{if } C_1 \text{ or } C_2 \text{ holds,} \\ 0 & \text{if } C_3 \text{ or } C_4 \text{ holds,} \\ a & \text{if } C_5 \text{ holds,} \end{cases} \quad (12)$$

where parameters $a \in \mathbb{R}_{0,+}$ and $b \in \mathbb{R}_+$ ($b > a$) describe the degree of non-volatility of the nano-structure and tunable conditions C_n ($n = 1, 2, 3, 4, 5$) are mathematically described by

$$\begin{aligned} C_1 = & \{(w \in (0, D) \text{ and} \\ & ((v > v_{t0}) \text{ or } (v < -v_{t1})))\}, \end{aligned} \quad (13)$$

$$\begin{aligned} C_2 = & \{(w = 0 \text{ and } v > v_{th0}) \\ & \text{or} \\ & (w = D \text{ and } v < -v_{th1})\}, \end{aligned} \quad (14)$$

$$C_3 = \{w = 0 \text{ and } v \leq v_{th0}\}, \quad (15)$$

$$C_4 = \{w = D \text{ and } v \geq -v_{th1}\}, \quad (16)$$

$$\begin{aligned} C_5 = & \{(w = \bar{w} \in (0, D) \text{ and} \\ & ((v \leq v_{t0}) \text{ and } (v \geq -v_{t1})))\}. \end{aligned} \quad (17)$$

In conditions (14)–(16) voltage parameters $v_{th0} \in \mathbb{R}_{0,+}$ and $v_{th1} \in \mathbb{R}_{0,+}$ represent the *boundary thresholds* (i.e. the thresholds the magnitude of the input needs to exceed, after a sign reversal, for the state to be released from the lower and upper bound respectively). As reported in [22], the introduction of such boundary thresholds was inspired by the following comment from Williams in [8]: “*the switching characteristic observed for a particular memristive system helps to classify the nature of the boundary conditions on the state variable of the device*”. Further voltage parameters $v_{t0} \in \mathbb{R}_{0,+}$ and $v_{t1} \in \mathbb{R}_{0,+}$ in (13) and (17) denote the *programmability thresholds* (i.e. the thresholds the magnitude of a positive and negative input respectively needs to exceed for the window function to exhibit a discontinuous transition from a smaller a to a larger b value). The introduction of these programmability thresholds [27] took inspiration from a recent comment from Prof. Eshraghian [28], which, rating a large class of memristor models available in literature, stated that “*the common problem in these models*

is that there is no threshold consideration, so there is a gap in knowledge base for design characterization.” In other words, a good memristor model should exhibit the activation threshold property of the evolution of the dynamics in order to reflect the degree of non-volatility of the memristor. This is particularly important in neuromorphic applications, where the model may be used to emulate the behavior of biological synapses.

The BCM model is one of the simplest memristor models available in literature (it possesses a closed-form solution for state w as function of flux φ under any input/initial condition combination [29]) and yet it may accurately capture nonlinear dynamics pertaining to various nano-structures irrespective of the physical mechanisms underlying the memristive behavior (thanks to its extreme versatility embedded in the boundary conditions (14)–(16) [22]) and even complex neural learning rules at the origin of primitive intelligence (thanks to its programming threshold capability expressed by conditions (13) and (17) [27]).

The optimization strategy of Section III shall sweep parameters a and b in (12) and thresholds v_{th0} , v_{th1} , v_{t0} and v_{t1} in (13)–(17).

Unlike models [18]–[22], the Team [23] models the memristor as the Pickett model (see Section II-A). The state equation is defined as

$$\frac{dw}{dt} = \begin{cases} k_{off} \left(\frac{i}{i_{off}} - 1 \right)^{\alpha_{off}} f_{off}(w) & \text{if } i > i_{off} > 0, \\ 0 & \text{if } i_{on} < i < i_{off}, \\ k_{on} \left(\frac{i}{i_{on}} - 1 \right)^{\alpha_{on}} f_{on}(w) & \text{if } i < i_{on} < 0, \end{cases} \quad (18)$$

where w is the state variable denoting, as in the Pickett model, the length of the tunnel barrier, $k_{off} \in \mathbb{R}_+$ and $k_{on} \in \mathbb{R}_-$ are factors with the same dimensions as velocity, $\alpha_{off} \in \mathbb{R}_+$ and $\alpha_{on} \in \mathbb{R}_+$ are constants, while $i_{off} \in \mathbb{R}_+$ and $i_{on} \in \mathbb{R}_-$ are current thresholds. Functions $f_{off}(w)$ and $f_{on}(w)$ are expressed as

$$\begin{aligned} f_{off}(w) &= \exp \left(-\exp \left(\frac{w - a_{off}}{w_c} \right) \right), \\ f_{on}(w) &= \exp \left(-\exp \left(\frac{a_{on} - w}{w_c} \right) \right), \end{aligned} \quad (19)$$

where $a_{off} \in \mathbb{R}_+$ and $a_{on} \in \mathbb{R}_+$ are coefficients with the same dimensions as space. The state variable w is constrained to lie within closed interval $[w_{on}, w_{off}]$, where a reasonable choice for the bounds is $w_{on} = a_{off}$ and $w_{off} = a_{on}$. The current-voltage relation may be mathematically described as

$$v = R_{on} \exp \left(\lambda \frac{w - w_{on}}{w_{off} - w_{on}} \right) i, \quad (20)$$

where $\lambda = R_{off} R_{on}^{-1}$ and R_{on} and R_{off} are expressed in Ω .

The values of parameters i_{off} and i_{on} in (18) respectively are $1 \mu\text{A}$ and $-1 \mu\text{A}$. On and off resistances R_{on} and R_{off} in equation (20) are set to 100Ω and $200 \text{k}\Omega$ respectively, while memristor initial state $w(0)$ is taken as 1.75 nm . The following parameters shall be swept in the optimization procedure of Section III: α_{off} , α_{on} , k_{off} , k_{on} (see equation (18)), a_{off} , a_{on} and w_c (see equations (18)–(19)).

As a final note before dealing with the optimization process, it is important to note that the state variable in the Pickett and in the TEAM models is the complement of the state variable in models [18]–[22] with respect to the entire length D of the nano-film. In the next section the symbol used for the normalized state is x .

III. Optimization Procedure

The optimization procedure carries out a multiple run of a combination of Simulated Annealing [24] and Gradient Descent algorithms [25]. Following Chua's theory [2], the most reasonable choices for the pair of memristor variables under optimization may involve either state and flux or charge and flux. We investigated the performance of several cost functions taking into account combinations of memristor state, memductance, charge, flux and

voltage. The most suitable cost function $e(\cdot, \cdot)$ for optimizing Joglekar's, Biodek's, Prodomakis' and the TEAM models is given by a combination of the root mean squared error of flux and state given by

$$e_{x,\varphi} = \sqrt{\frac{\sum_{n=1}^N (x_{m,n} - \bar{x}_r)^2}{\bar{x}_r^2}} + \sqrt{\frac{\sum_{n=1}^N (\varphi_{m,n} - \bar{\varphi}_r)^2}{\bar{\varphi}_r^2}}. \quad (21)$$

Optimizing the BCM model with respect to this cost function did not lead to an improvement in the shape of the pinched hysteresis loop of the current-voltage characteristic compared to the reference given in [16]. Therefore, we optimized the parameters of the BCM model with respect to the cost function

$$e_{q,\varphi} = \sqrt{\frac{\sum_{n=1}^N (q_{m,n} - \bar{q}_r)^2}{\bar{q}_r^2}} + \sqrt{\frac{\sum_{n=1}^N (\varphi_{m,n} - \bar{\varphi}_r)^2}{\bar{\varphi}_r^2}}, \quad (22)$$

i.e. a combination of the root mean squared error of charge and flux. In both (21) and (22), the index r indicates the reference time series, the index m is used for the time series of the model to be optimized. A barred variable denotes the time average of the variable samples.

In Joglekar's model the sweep concerns parameter p in (9). Its initial value is set to 1. We swept p in the range of $0 \leq p \leq 100$. The value found after an optimization procedure was $p_{\text{opt}} = 9.88$. No improvement in the pinched hysteresis loop nor in the shape or range of the temporal evolution of the memristor state and flux variables could be observed.

For Prodomakis' model, parameters considered for the optimization procedure were p (with $p = 1$ as initial value) and j (initial value $j = 1.6$). The parameters were optimized in a range of $0 \leq p \leq 100$ and $-100 \leq j \leq 100$. The optimized parameter set is found to be $p_{\text{opt}} = 99.94$ and $j_{\text{opt}} = -44.37$. Again, no improvement in the hysteresis loop nor in the temporal evolution of the memristor state and flux variables could be observed.

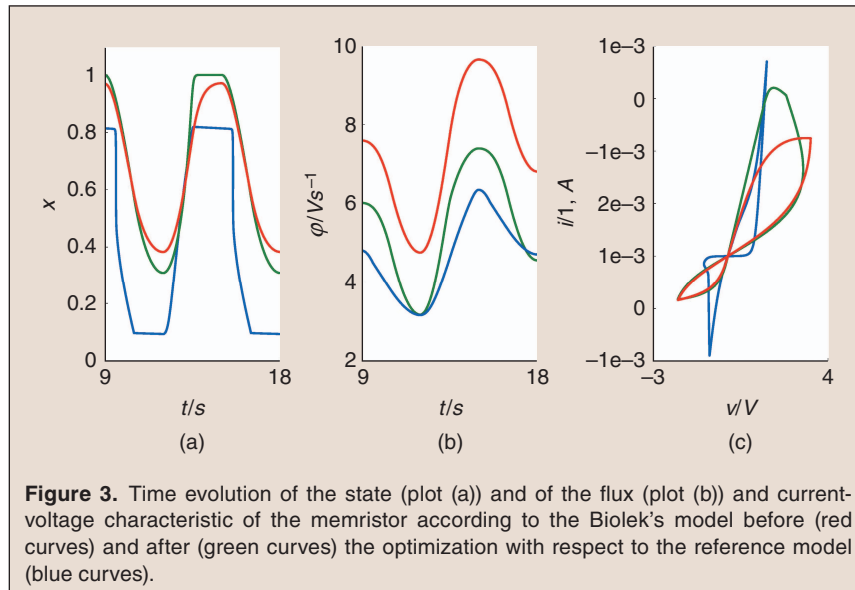


Figure 3. Time evolution of the state (plot (a)) and of the flux (plot (b)) and current-voltage characteristic of the memristor according to the Biodek's model before (red curves) and after (green curves) the optimization with respect to the reference model (blue curves).

Table 2.
Initial (step (1)) and optimized (step (2)) parameters of the BCM model.
Threshold voltages are expressed in V.

Step	$V_{\text{th}0}$	$V_{\text{th}1}$	$V_{\text{f}0}$	$V_{\text{f}1}$	a	b
(1)	0.2	0.35	0.15	0.15	$1 \cdot 10^{-5}$	1
(2)	4.7401	2.4629	0.9150	1.3048	0.1494	1.6182

Therefore neither Joglekar's nor Prodomakis' models were able to reproduce the dynamics shown by the reference model - neither with the initial parameter values nor with optimized parameters.

In the case of Biolek's model the optimization procedure sweeps parameter p in (10). Its initial and optimized values respectively are 1 and 6. A comparison between reference model and initial and optimized Biolek's model may be found in Fig. 3.

The BCM model offers the opportunity to tune a large number of parameters, namely constants defining the degree of non-volatility, i.e. a and b in (12), threshold voltages at boundaries, i.e. v_{th0} and v_{th1} in boundary conditions (14)–(16), and programming threshold voltages, i.e. v_{t0} and v_{t1} in (13) and (17). The initial and optimized values of these parameters are reported in Table 2. A comparison between reference model and initial and optimized BCM model may be found in Fig. 4.

In the case of the TEAM model the parameters under tuning are α_{off} , α_{on} , k_{off} and k_{on} in (18) and a_{off} , a_{on} and w_c in (19). Table 3 reports the initial and optimized values of these parameters. A comparison between reference model and initial and optimized TEAM model may be found in Fig. 5.

A. Comparison of the Effect of Optimization on Different Models

In order to compare the effect of a parameter optimization on different models with respect to the pinched hysteresis loop in the i - v -plane, we calculated the relative root mean squared error with respect to the voltage- and current- time series given by Biolek's, TEAM, and BCM models. The error is given by

$$e_{v,i} = \sqrt{\frac{1}{N} \left(\sum_{n=1}^N (v_{m,n} - \bar{v}_r)^2 + \sum_{n=1}^N (i_{m,n} - \bar{i}_r)^2 \right)}, \quad (23)$$

where again barred variables denote the time average of the variable samples, the index r indicates reference time series and the index m is used to indicate model time series.

Here, we use a relative root mean square error in order to be able to give an intuitive measure for the model quality. For the BCM model, the initial parameters give an error of $e_{v,i} = 0.4201$. After parameter

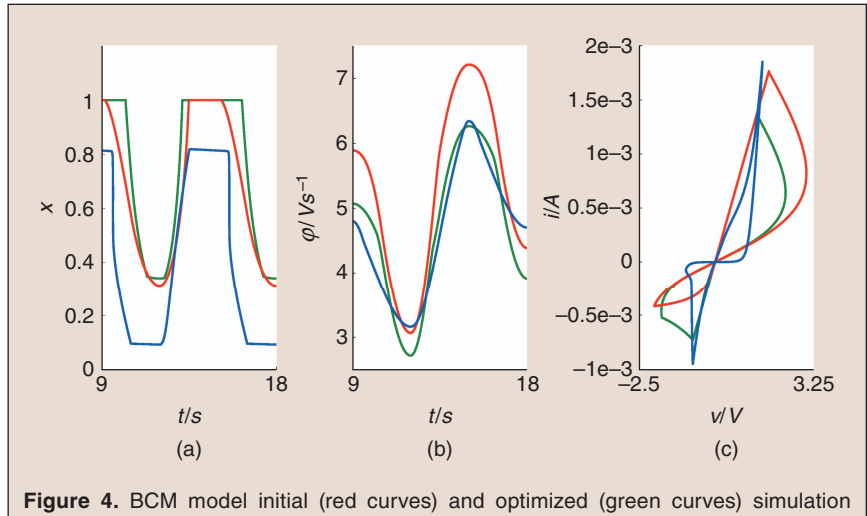


Figure 4. BCM model initial (red curves) and optimized (green curves) simulation results and Pickett model predictions (blue curves). Plot (a): state versus time; Plot (b): flux versus time; Plot (c): current versus voltage.

optimization with respect to the cost function in equation (22), the error $e_{v,i} = 0.3358$ may be obtained. For the TEAM model, the error for the initial parameters suggested in [23] is $e_{v,i} = 0.8342$. A parameter optimization with respect to cost function (21) leads to an improved performance of the model indicated by the error $e_{v,i} = 0.3808$ – less than half of the initial error.

For Biolek's model, an initial error of $e_{v,i} = 0.4521$ using the initial parameter value $p = 1$ may be calculated. For the optimized value of $p = 6$ according to cost function (21), an error value of $e_{v,i} = 0.4256$ shows that even though the shape and range of the state and flux time series may be improved by an optimization process, the shape of the pinched hysteresis loop may not be considerably enhanced by an optimization procedure.

This indicates that while all suggested models can benefit from an optimization of the parameters

Table 3.
Initial (step (1)) and optimized (step (2)) values of α_{off} , α_{on} , k_{off} and k_{on} in (18) and of a_{off} , a_{on} and w_c in (19). The dimensional units of k_{off} and k_{on} are ms^{-1} , while a_{on} , a_{off} and w_c are expressed in m .

Parameter	Step (1)	Step (2)
α_{off}	3	1.7747
α_{on}	3	3.3849
k_{off}	$8 \cdot 10^{-13}$	$7.2794 \cdot 10^{-13}$
k_{on}	$-8 \cdot 10^{-13}$	$-8.1661 \cdot 10^{-13}$
a_{off}	$1.2 \cdot 10^{-9}$	$8.0720 \cdot 10^{-10}$
a_{on}	$2.3 \cdot 10^{-9}$	$2.2579 \cdot 10^{-9}$
w_c	$1.07 \cdot 10^{-9}$	$3.5618 \cdot 10^{-10}$

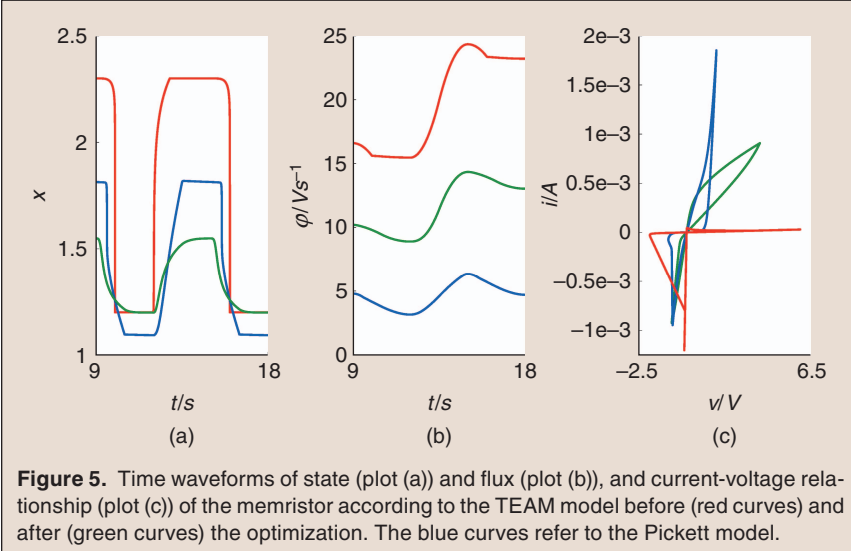


Figure 5. Time waveforms of state (plot (a)) and flux (plot (b)), and current-voltage relationship (plot (c)) of the memristor according to the TEAM model before (red curves) and after (green curves) the optimization. The blue curves refer to the Pickett model.

to the actual circuit under investigation, the parameter set of the BCM model and Bielek's model seem to be less dependent on the actual design of the circuit under investigation. Accordingly, those models benefit less from an optimization of parameters. However, for the circuit and optimization procedure studied here, the BCM model shows the lowest error with respect to the v-i-characteristics most relevant for circuit design.

Here it is important to note that the variability range of the state variable depends on the actual memristor model under consideration. In Joglekar's, Prodomakis' and Bielek's models as well as in the BCM model the state variable denotes the width of the conductive layer and may assume values in $[0, D]$, where D is the full length of the nano-device. In the Pickett's model, as well as in the TEAM model, the state variable is the tunnel barrier width of the nano-structure and may range from $[w_{\text{on}}, w_{\text{off}}]$. Furthermore, the state variable in the first set of models is the complement of the state variable in the latter set of models with respect to the entire length of the memristor. This differences in the models explain a shift of the state variable curves in Figs. 4 and 5.

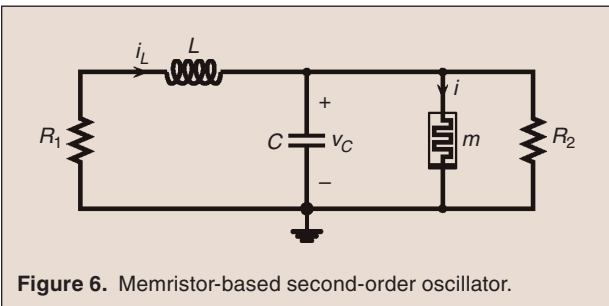


Figure 6. Memristor-based second-order oscillator.

IV. Case Studies

This section shall study the variance of the dynamics of basic memristor-based circuits on the basis of the memristor model under use. Here we shall only consider those models which, according to the optimization procedure of Section III, exhibit good capability in tracking the dynamics of the reference model. As a result, Joglekar's model and Prodomakis' model shall not be considered any further.

A. Second-Order Circuit

The first circuit under test is the second-order oscillator shown

in Fig. 6. This oscillator, inspired from the oscillator presented in [30] and later analytically studied in [10], presents an extra resistor R_2 in parallel with the memristor (the other resistor, R_1 , is negative). Application of Kirchhoff's Laws to the circuit of Fig. 6 yields the following ordinary differential equations for the rate of change of the first two state variables, defined as $x_1 = v_C$ and $x_2 = -R_1 i_L$:

$$\frac{dx_1}{dt} = \left(x_2 + x_1 \left(\frac{1}{M(x_3)} + \frac{1}{R_2} \right) R_1 \right) \quad (24)$$

$$\frac{dx_2}{dt} = \alpha (x_2 - x_1), \quad (25)$$

where $\tau = tt_0^{-1}$ is the normalized time variable with normalization factor $t_0 = -CR_1$, while $\alpha = CR_1^2L^{-1}$. The other state equation, governing the time evolution of state x_3 of memristor m with memristance $M(x_3)$, has a different expression according to the memristor model under use, i.e.

$$\frac{dx_3}{d\tau} = -CR_1 \frac{\mu R_{\text{on}}}{D^2} \frac{x_1}{M(x_3)} f(x_3, x_1), \quad (26)$$

for Bielek's and the BCM models (the window function $f(\cdot, \cdot)$ is respectively defined in (10) and (12), $x_3 = wD^{-1}$, where w denotes the length of the conductive layer and D is the full longitudinal extension of the nano-device, and the expression for the memristance $M(\cdot)$ is given in (5)) and

$$\frac{dx_3}{d\tau} = \begin{cases} t_0 k_{\text{off}} \left(\frac{i}{i_{\text{off}}} - 1 \right)^{\alpha_{\text{off}}} f_{\text{off}}(x_3) & \text{if } i > i_{\text{off}} > 0, \\ 0 & \text{if } i_{\text{on}} < i < i_{\text{off}}, \\ t_0 k_{\text{on}} \left(\frac{i}{i_{\text{on}}} - 1 \right)^{\alpha_{\text{on}}} f_{\text{on}}(x_3) & \text{if } i < i_{\text{on}} < 0, \end{cases}$$

for the TEAM model ($x_3 = w$, where w indicates the tunnel barrier, $i = x_1 M(x_3)^{-1}$, the memristance function may be derived from (20), while the expressions for $f_{\text{off}}(\cdot)$ and $f_{\text{on}}(\cdot)$ are given in (19)).

In the transient simulations to follow the circuit parameters are set as $R_1 = -50 \Omega$, $L = 10 \text{ mH}$ and $C = 1 \mu\text{F}$ and $R_2 = 250 \Omega$. The initial conditions for the first two state variables were set to $x_1(0) = 10 \text{ mV}$ and $x_2(0) = 500 \text{ mV}$ (meaning $i_L(0) = 10 \text{ mA}$). The initial and final instants of normalized time τ were taken as 0 and 2000 respectively, while the normalized time step $\Delta\tau$ was chosen as $1 \cdot 10^{-1}$. This corresponds to initial and final instants of time t respectively equal to 0s and 0.1s and to a time step Δt equal to 5 μs , since $t_0 = 50 \mu\text{s}$.

The parameters of the reference model were set as follows: $\phi_o = 0.95 \text{ eV}$, $L_m = 0.0998 \text{ eVm}$, $w_1 = 0.1261 \cdot 10^{-9} \text{ m}$, $f_{\text{off}} = 8.17175 \cdot 10^{-13} \text{ ms}^{-1}$, $i_{\text{off}} = 100 \mu\text{A}$, $a_{\text{off}} = 1.2 \cdot 10^{-9} \text{ m}$, $f_{\text{on}} = 8 \cdot 10^{-13} \text{ ms}^{-1}$, $i_{\text{on}} = 100 \mu\text{A}$, $a_{\text{on}} = 2.3 \cdot 10^{-9} \text{ m}$, $b = 100 \cdot 10^{-6} \text{ A}$, $w_c = 107 \cdot 10^{-12} \text{ m}$, $R_s = 50 \Omega$, $x_3(0) = 2.3 \cdot 10^{-9} \text{ m}$. Under such parameter setting, the memristor-based circuit of Fig. 6 experienced oscillations at frequency $f = 1.3605 \text{ kHz}$.

The common parameters of Biolek's model and of the BCM model were set to $\mu = 1 \cdot 10^{-11} \text{ m}^2 \text{ V}^{-1} \text{ s}^{-1}$, $D = 10 \cdot 10^{-9} \text{ m}$, $R_{\text{on}} = 100 \Omega$, $R_{\text{off}} = 3.68 \text{ k}\Omega$ and $x_3(0) = 0 \text{ m}$. Setting parameter p in Biolek's window (10) to 1, a transient simulation revealed the development of oscillations at frequency $f = 1.4085 \text{ kHz}$.

In the BCM model the window parameters were specified as follows: $a = 1$, $b = 1$, $v_{\text{th}0} = 0 \text{ V}$, $v_{\text{th}1} = 0 \text{ V}$, $v_{r0} = 0 \text{ V}$ and $v_{rl} = 0 \text{ V}$. The autonomous system was found to exhibit an oscillation at frequency $f = 1.4286 \text{ kHz}$.

Finally in the TEAM model the parameters were set to $\alpha_{\text{off}} = 3$, $k_{\text{off}} = 8 \cdot 10^{-13} \text{ ms}^{-1}$, $i_{\text{off}} = 1 \mu\text{A}$, $a_{\text{off}} = 1.2 \cdot 10^{-9} \text{ m}$, $\alpha_{\text{on}} = 3$, $k_{\text{on}} = -8 \cdot 10^{-13} \text{ ms}^{-1}$, $i_{\text{on}} = -1 \mu\text{A}$, $a_{\text{on}} = 2.3 \cdot 10^{-9} \text{ m}$, $w_c = 107 \cdot 10^{-11} \text{ m}$, $x_{\text{on}} = a_{\text{off}}$, $x_{\text{off}} = a_{\text{on}}$, $R_{\text{on}} = 150 \Omega$, $R_{\text{off}} = 10 \text{ k}\Omega$ and $x(0) = 2.3 \cdot 10^{-9} \text{ m}$. The oscillation frequency predicted by the TEAM model is $f = 1.3793 \text{ kHz}$.

The oscillatory time waveforms of x_1 (in solid-line style) and x_3 (in dashed-line style) are shown in Fig. 7, while the limit cycle on the $x_1 - x_2$ state plane is shown in Fig. 8. Curves in blue, black, red and green respectively refer to the Pickett's model, to Biolek's model, to the BCM model and to the TEAM model.

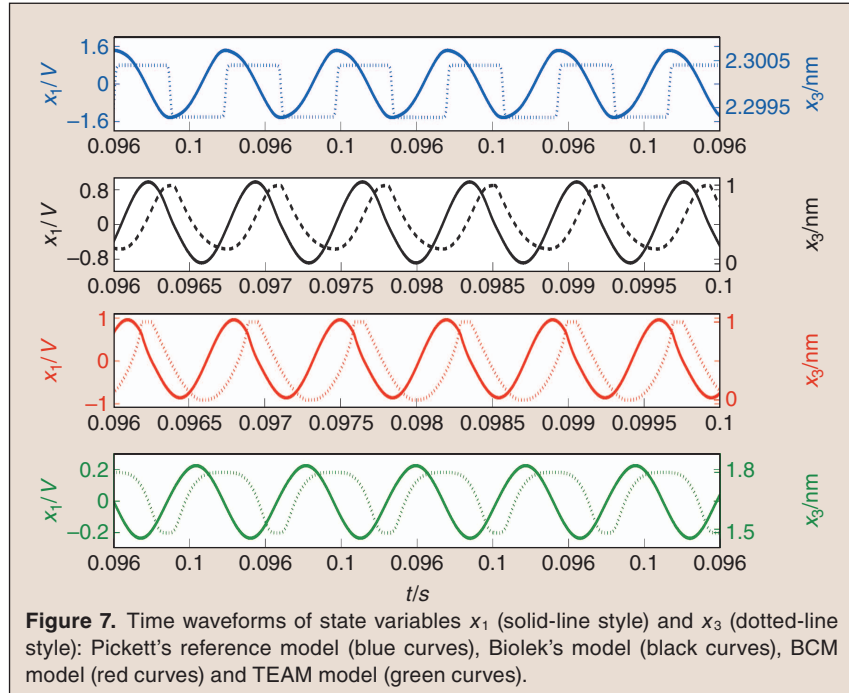


Figure 7. Time waveforms of state variables x_1 (solid-line style) and x_3 (dotted-line style): Pickett's reference model (blue curves), Biolek's model (black curves), BCM model (red curves) and TEAM model (green curves).

Fig. 9, showing the Fast Fourier Transform of the time signal $x_1(t)$, highlights the better accuracy of the TEAM model in capturing the higher-order harmonics of the signal referring to the Pickett's model. Nonetheless the simpler Biolek's and BCM model are able to capture the first harmonic component in the reference signal.

Figs. 10 (time behavior of state variable x_1) and 11 (time behavior of state variable x_2) show for each memristor model the response of the circuit of

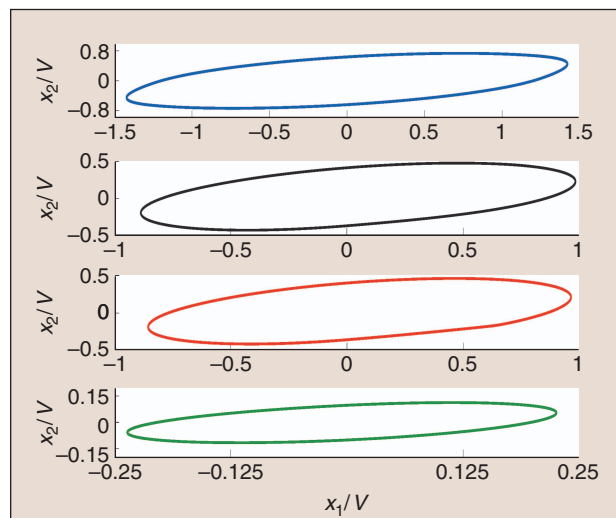


Figure 8. Limit cycle on state plane $x_1 - x_2$: Pickett's reference model (in blue color), Biolek's model (in black color), the BCM model (in red color) and the TEAM model (in green color).

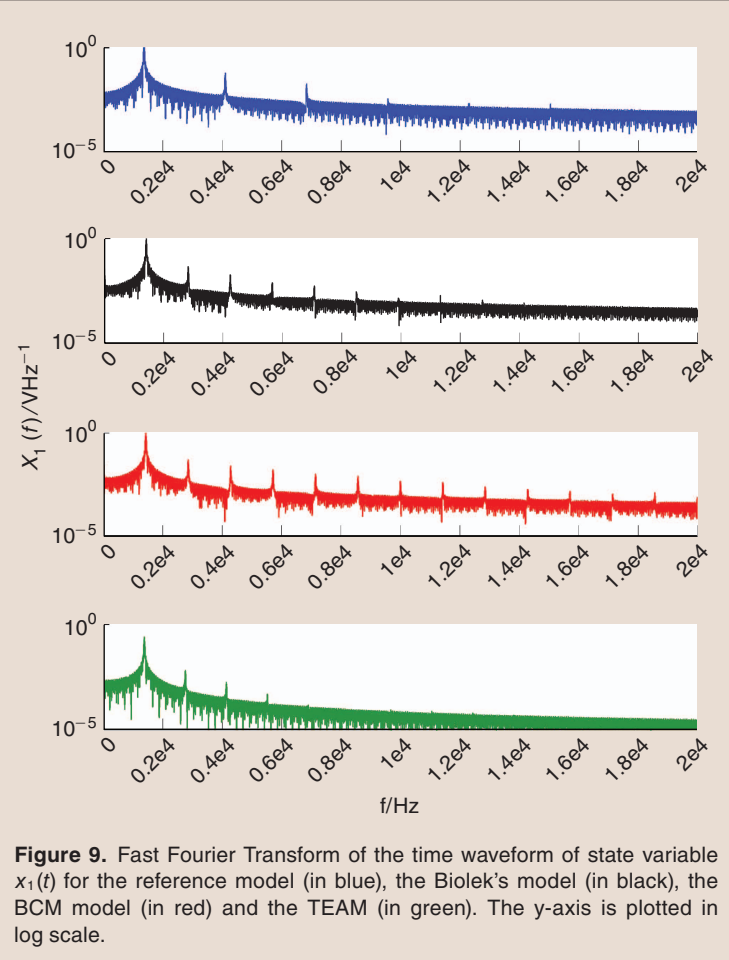


Figure 9. Fast Fourier Transform of the time waveform of state variable $x_1(t)$ for the reference model (in blue), the Biolek's model (in black), the BCM model (in red) and the TEAM (in green). The y-axis is plotted in log scale.

Fig. 6 to a current pulse source inserted in parallel to capacitor C and injecting current into its upper node. Let us assume that this current pulse, let us call it i_p , is characterized by amplitude i_0 , time delay t_d , rise time t_r , fall time t_f and width Δt . It may thus be defined as

$$i_p(\tau) = \begin{cases} 0 & \text{if } \tau < \tau_0 \mid \tau > \tau_3 \\ \frac{i_0}{\tau_1 - \tau_0}(\tau - \tau_0) & \text{if } \tau_0 \leq \tau \leq \tau_1 \\ i_0 & \text{if } \tau_1 < \tau < \tau_2 \\ i_0 - \frac{i_0}{\tau_3 - \tau_2}(\tau - \tau_2) & \text{if } \tau_2 \leq \tau \leq \tau_3, \end{cases} \quad (27)$$

where $\tau_0 = t_d t_0^{-1}$, $\tau_1 = (t_d + t_r) t_0^{-1}$, $\tau_2 = (t_d + t_r + \Delta t) t_0^{-1}$ and $\tau_3 = (t_d + t_r + \Delta t + t_f) t_0^{-1}$. The addition of this input to the circuit of Fig. 6 changes equations (24)–(25) into the following equations:

$$\frac{dx_1}{dt} = t_0 \left(i_p - \frac{1}{R_1} x_2 - \frac{1}{M(x_3) x_1 - \frac{1}{R_2} x_1} \frac{1}{C} \right), \quad (28)$$

$$\frac{dx_2}{dt} = t_0 (x_2 - x_1) \frac{-R_1}{L}. \quad (29)$$

The system becomes non-autonomous and the numerical integration of differential equations (28)–(29) and (26) (for Biolek's and the BCM model) or (27) (for the TEAM model) is best carried out by setting the time normalization factor to $t_0 = 1$ s. The parameters of the reference model and of the three models under comparison are left unvaried with respect to the simulation scenario in Fig. 7.

It turns out that Biolek's model and the BCM model present a transient response similar to the response of the reference model. On the other hand, the TEAM model predicts the development of an oscillation with smaller amplitude.

B. Third-Order Circuit

The next case study refers to a memristor-based version of the third-order canonical Chua's oscillator, employing two identical memristors in anti-parallel in place of Chua's diode and shown in Fig. 12. Applying Kirchhoff's Laws to this circuit, after some algebraic manipulation, the first three state equations of the autonomous dynamical system defining the rate of change for state variables $x_1 = v_{C1}$, $x_2 = v_{C2}$ and $x_3 = -R_{IL}$ may be written as it follows:

$$\begin{aligned} \frac{dx_1}{d\tau} &= -\alpha \left(\frac{R}{M(x_4)} + \frac{R}{M(x_5)} + \frac{R}{R_{N2}} \right) x_1 - \alpha x_3, \\ \frac{dx_2}{d\tau} &= \gamma x_2 + x_3, \\ \frac{dx_3}{d\tau} &= \beta (-x_3 + x_1 - x_2), \end{aligned} \quad (30)$$

where $\tau = t t_0^{-1}$ is the normalized time variable with normalization factor $t_0 = RC_2$, while $\alpha = C_2 C_1^{-1}$, $\beta = R^2 C_2 L^{-1}$ and $\gamma = -RR_{N1}^{-1}$. The other two state equations, governing the time evolution of state variables x_4 and x_5 , respectively denoting the states of memristors m_1 and m_2 with memristances $M(x_4)$ and $M(x_5)$, have different expressions according to the memristor model under use, i.e.

$$\begin{aligned} \frac{dx_4}{d\tau} &= \frac{\mu R_{on} t_0}{D^2} \frac{x_1}{M(x_4)} f(x_4, x_1), \\ \frac{dx_5}{d\tau} &= \frac{\mu R_{on} t_0}{D^2} \frac{-x_1}{M(x_5)} f(x_5, -x_1), \end{aligned} \quad (31)$$

for Biolek's model and the BCM model (the window function $f(\cdot, \cdot)$ is respectively defined in (10) and (12), $x_4 = w_1 D^{-1}$, $x_5 = w_2 D^{-1}$, where w denotes the length of the conductive layer and D stands for the full longitudinal extension of the nano-device, and the expression for the memristance $M(\cdot)$ may be derived from (5)) and

$$\begin{aligned} \frac{dx_4}{d\tau} &= \begin{cases} t_0 k_{\text{off}} \left(\frac{i_1}{i_{\text{off}}} - 1 \right)^{\alpha_{\text{off}}} f_{\text{off}}(x_4) & \text{if } i_1 > i_{\text{off}} > 0, \\ 0 & \text{if } i_{\text{on}} < i_1 < i_{\text{off}}, \\ t_0 k_{\text{on}} \left(\frac{i_1}{i_{\text{on}}} - 1 \right)^{\alpha_{\text{on}}} f_{\text{on}}(x_4) & \text{if } i_1 < i_{\text{on}} < 0, \end{cases} \\ \frac{dx_5}{d\tau} &= \begin{cases} t_0 k_{\text{off}} \left(\frac{-i_2}{i_{\text{off}}} - 1 \right)^{\alpha_{\text{off}}} f_{\text{off}}(x_5) & \text{if } -i_2 > i_{\text{off}} > 0, \\ 0 & \text{if } i_{\text{on}} < -i_2 < i_{\text{off}}, \\ t_0 k_{\text{on}} \left(\frac{-i_2}{i_{\text{on}}} - 1 \right)^{\alpha_{\text{on}}} f_{\text{on}}(x_5) & \text{if } -i_2 < i_{\text{on}} < 0, \end{cases} \quad (32) \end{aligned}$$

for the TEAM model ($x_4 = w_1$, $x_5 = w_2$, where w indicates the tunnel barrier width of the nano-device, $i_1 = x_1 M(x_4)^{-1}$, $i_2 = x_1 M(x_5)^{-1}$, the memristance function may be derived from (20), while the expressions for $f_{\text{off}}(\cdot)$ and $f_{\text{on}}(\cdot)$ are given in (19)).

In the simulations to follow all the circuit elements in Fig. 12 except for capacitor C_1 are set to the following values: $R = 300 \Omega$, $R_{N2} = -952.38 \text{ k}\Omega$, $C_2 = 60 \text{ nF}$, $L = 100 \text{ mH}$, $R_{N1} = -2 \text{ k}\Omega$. The initial conditions on the first three state variables were chosen as $x_1(0) = 6 \text{ mV}$, $x_2(0) = 20 \text{ mV}$ and $x_3(0) = -0.3 \text{ V}$ (meaning $i_L(0) = 1 \text{ mA}$). In the numerical integration of state equations (30) and (31) (for Biolek's and the BCM models) or (32) (for the TEAM model) the normalized time variable τ was swept from 0 to 100000 with step 0.1. This corresponds to sweeping time variable t from 0 s to 1.8 s with step $1.8 \mu\text{s}$.

The reference model parameters are specified as it follows: $\phi_o = 0.95e \text{ V}$, $L_m = 0.0998e \text{ Vm}$, $w_1 = 0.1261 \cdot 10^{-9} \text{ m}$, $f_{\text{off}} = 1.05 \cdot 10^{-11} \text{ ms}^{-1}$, $i_{\text{off}} = 100 \mu\text{A}$, $a_{\text{off}} = 1.2 \cdot 10^{-9} \text{ m}$, $f_{\text{on}} = 1 \cdot 10^{-11} \text{ ms}^{-1}$, $i_{\text{on}} = 100 \mu\text{A}$, $a_{\text{on}} = 2.3 \cdot 10^{-9} \text{ m}$, $b = 5000 \cdot 10^{-6} \text{ A}$, $w_c = 107 \cdot 10^{-10} \text{ m}$ and $R_s = 85 \Omega$. Under these parameter settings, the memristor-based circuit of Fig. 12 experiences chaotic oscillations for $C_1 = 55 \text{ nF}$. A double-scroll attractor may be observed in the $x_1 - x_2 - x_3$ state space (see Fig. 13).

Let us keep the circuit components of the memristor-based Chua's canonical oscillator unvaried and study the effect of the memristor model on the dynamical behavior of the circuit. The common parameters of Biolek's model and of the BCM model were set to: $\mu = 1 \cdot 10^{-11} \text{ m}^2 \text{ V}^{-1} \text{ s}^{-1}$, $D = 10 \text{ nm}$, $R_{\text{on}} = 100 \Omega$ and $R_{\text{off}} = 5.9 \text{ k}\Omega$. The initial conditions on the last two state variables were chosen as $x_4(0) = 0 \text{ m}$ and $x_5(0) = 0 \text{ m}$. In Biolek's window function p was taken as 100. Under such simulation

settings chaos arises in the memristor-based Chua's canonical oscillator for $C_1 = 56 \text{ nF}$. The third-order autonomous system converges to the chaotic attractor shown in Fig. 14. The BCM model captures a similar chaotic behavior for the same value of C_1 , i.e. for $C_1 = 56 \text{ nF}$. This is demonstrated in Fig. 15, referring to the following choice for the tunable parameters of the BCM model's window function: $v_{\text{th}0} = 0 \text{ V}$, $v_{\text{th}1} = 0 \text{ V}$, $a = 1$, $b = 1$, $v_{l0} = 0 \text{ V}$ and $v_{l1} = 0 \text{ V}$.

The values of the parameters of the TEAM model were selected as follows: $\alpha_{\text{off}} = 3$, $k_{\text{off}} = 8 \cdot 10^{-8} \text{ ms}^{-1}$,

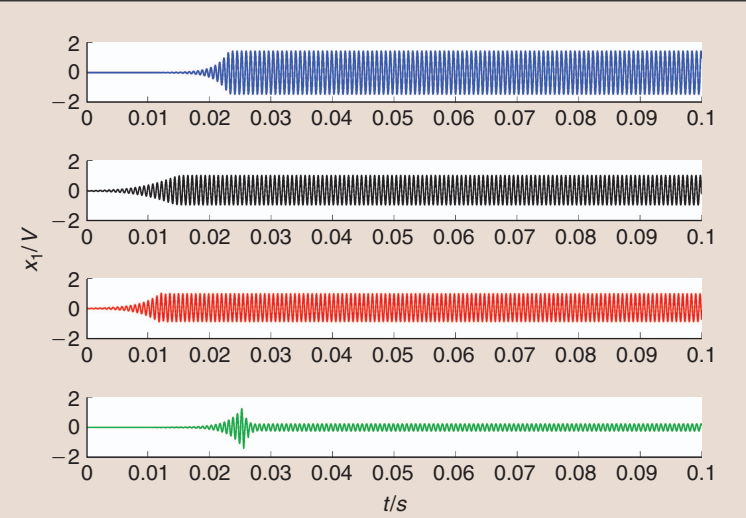


Figure 10. Response of the circuit of Fig. 6 to a current pulse: time waveform of x_1 for the reference model (in blue), the Biolek's model (in black), the BCM model (in red) and the TEAM (in green). The initial conditions on state x_1 and x_2 are set to 0 V, while the memristor is initially in the off-state. The current pulse parameters are $i_0 = 1 \mu\text{A}$, $t_d = 1 \text{ ms}$, $t_r = t_f = 1 \text{ ms}$ and $\Delta t = 10 \text{ ms}$.

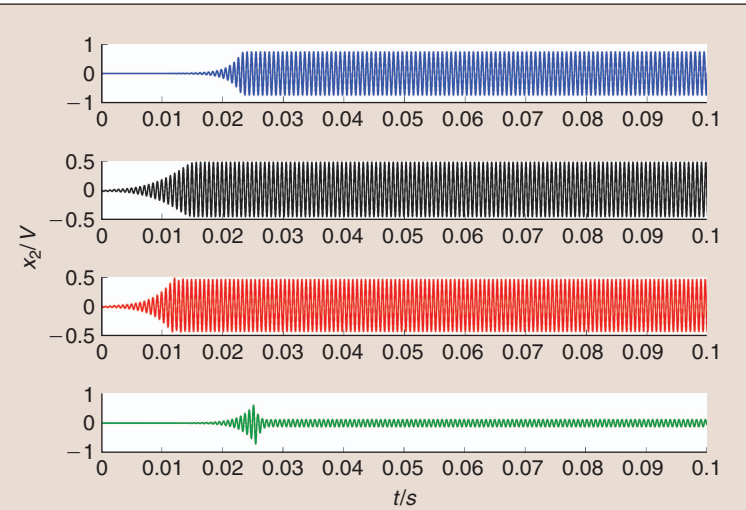


Figure 11. Time waveform of x_2 for the reference model (in blue), the Biolek's model (in black), the BCM model (in red) and the TEAM (in green) under the simulation scenario described in Fig. 10.

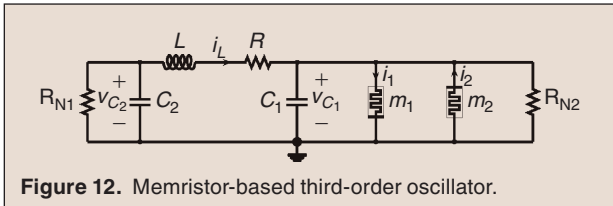


Figure 12. Memristor-based third-order oscillator.

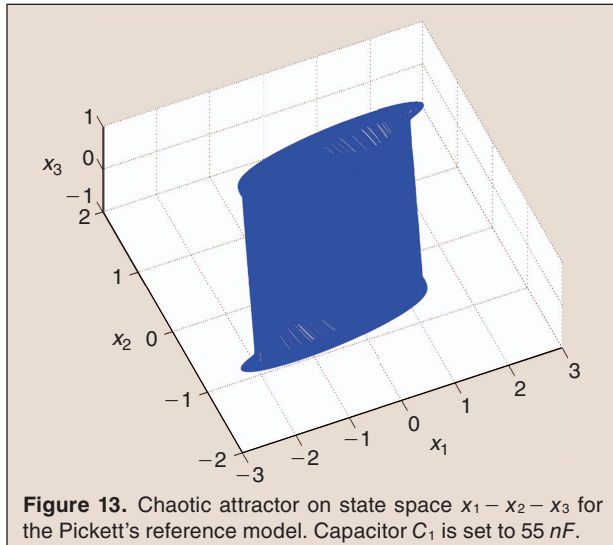


Figure 13. Chaotic attractor on state space $x_1 - x_2 - x_3$ for the Pickett's reference model. Capacitor C_1 is set to 55 nF.

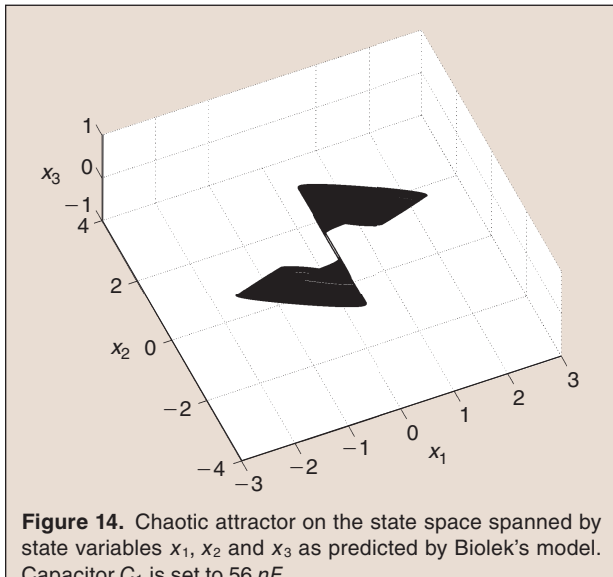


Figure 14. Chaotic attractor on the state space spanned by state variables x_1 , x_2 and x_3 as predicted by Biolek's model. Capacitor C_1 is set to 56 nF.

$i_{\text{off}} = 1 \mu\text{A}$, $a_{\text{off}} = 1.2 \cdot 10^{-9} \text{ m}$, $\alpha_{\text{on}} = 3$, $k_{\text{on}} = -8 \cdot 10^{-8} \text{ ms}^{-1}$, $i_{\text{on}} = -1 \mu\text{A}$, $a_{\text{on}} = 2.3 \cdot 10^{-9} \text{ m}$, $w_c = 107 \cdot 10^{-11} \text{ m}$, $x_{\text{on}} = a_{\text{off}}$, $x_{\text{off}} = a_{\text{on}}$, $R_{\text{on}} = 1 \text{ k}\Omega$ and $R_{\text{off}} = 1 \text{ M}\Omega$. The initial conditions for the states of the two memristors were set to $x_4(0) = x_5(0) = 2.3 \cdot 10^{-9} \text{ m}$. Numerical integration of the state equations (30) and (32) yields chaotic behavior for $C_1 = 52 \text{ nF}$. The chaotic attractor, shown in Fig. 16,

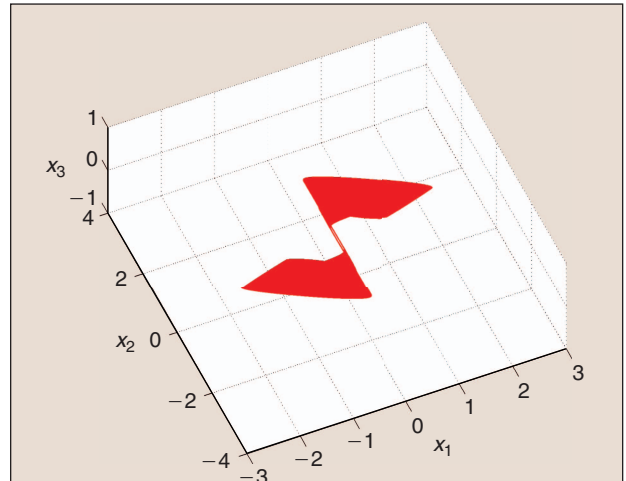


Figure 15. Chaotic attractor according to the BCM model. Capacitor C_1 is set to 56 nF.

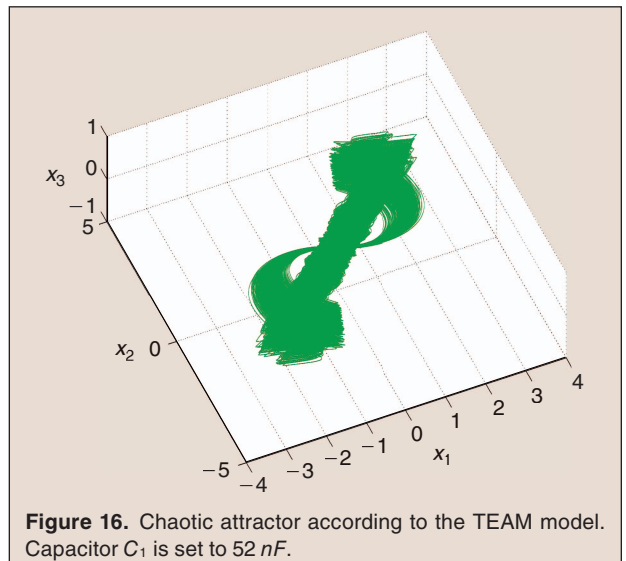


Figure 16. Chaotic attractor according to the TEAM model. Capacitor C_1 is set to 52 nF.

considerably differs from the two depicted in Figs. 14 and 15.

In order to prove the occurrence of chaotic behavior in all cases, we computed the Fast Fourier Transform of time signal $x_1(t)$. The results of this investigation are shown in Fig. 17 for the reference (blue curve), Biolek's (black curve), the BCM model (red curve) and the TEAM (green curve) models respectively. The observation of a wide frequency spectrum confirms the expectations.

In conclusion, Biolek's and the BCM models exhibit chaotic behavior for nearly the same value of capacitor C_1 as in the case of the reference model (56 nF versus 55 nF respectively). The TEAM model experiences chaotic behavior for a smaller capacitor value (52 nF). Nonetheless all the models under comparison

yield chaotic attractors which do not resemble the Pickett's model-based chaotic attractor. This dependence of the dynamical behavior of the memristor-based circuit of Fig. 12 upon the memristor model under use should serve as a warning to the circuit designer against a blind trust in the simulation results derived by means of any of the memristor models introduced in the literature. Memristor-based circuit design may not leave aside the preliminary development of a universal memristor model, independent upon the circuit to be used into and upon the excitation to be driven by.

V. Model Comparison and Discussion

This section briefly summarizes the comparison among the main memristor models considered in this manuscript (the Biolek's model, the BCM model and the TEAM model) and the Pickett model (reference model). The results are drawn from the test circuit and the nonlinear circuits presented in the sections III and IV, respectively. In particular, the following case-studies have been considered:

- *Test 1:* This test aims to identify which memristor model fits better the $i - v$ characteristic observed in the Pickett model under a particular triangular excitation (see figures 1 and 2).
- *Test 2:* In this case a memristor-based nonlinear circuit (see Fig. 6) with periodic behavior is considered. The qualitative comparison among the memristor models is based upon the following properties:
 - frequency of the limit cycle
 - frequency spectrum of the memristor voltage
 - transitory response due to an external pulse.
- *Test 3:* In this case a chaotic memristor-based nonlinear circuit is considered (see Fig. 12). Due to the complexity of the memristor models, it is not easy to compute the Lyapunov exponents of the chaotic attractors. The comparison is based on the appearance of the chaotic attractor in the state-space and their frequency spectra.

The results in the different tests are:

- *Result Test 1:* The optimization strategy (based upon a combination of Simulated Annealing and Gradient Descent methods) reveals that Biolek's model, the BCM model and the TEAM model reproduce the memristive dynamics of the

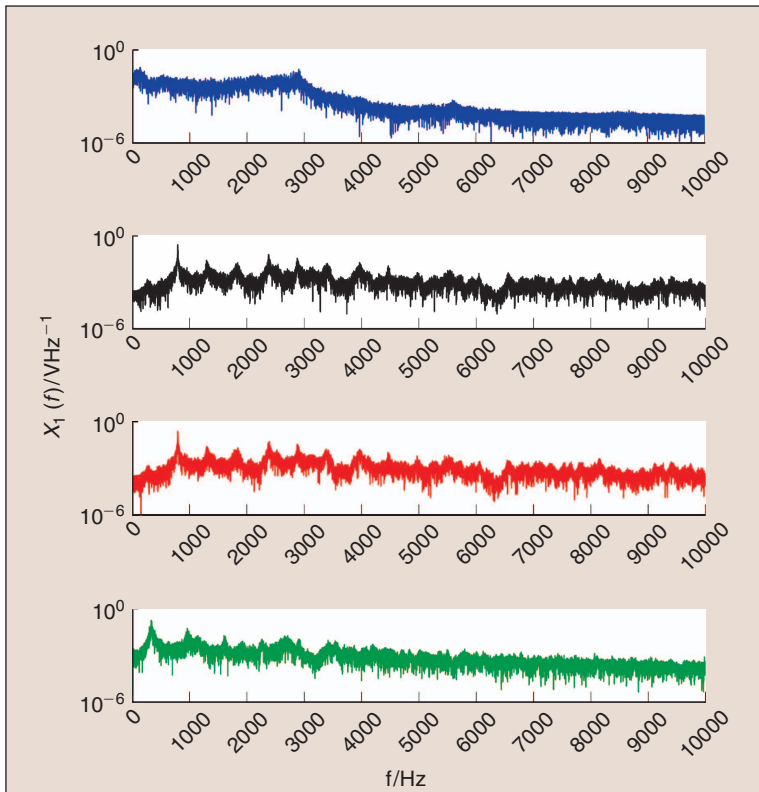


Figure 17. Frequency spectrum of the time signal $x_1(t)$ for the Pickett's reference model (in blue), Biolek's model (in black), the BCM model (in red) and the TEAM (in green).

reference model more accurately than the other models. The advantage of the first two models lies in their simplicity, despite they are not based on Simmons' electric tunnel effect [26]. Moreover, the BCM model is the only model for which a closed-form expression for the memristor state-flux relationship may be given under any input and initial condition combination [22]. In addition, for the circuit and optimization procedure considered in this manuscript, the BCM model shows the lowest error with respect to the v-i-characteristics most relevant for circuit design (see *Test 1* in Table 4). The TEAM model reflects Simmons' physical model, but, on the other hand, has a more complex mathematical formulation and an higher error with respect to the v-i characteristics. For a quantitative measure of comparison the interested reader may found details in Sect. III-A.

- *Result Test 2:* As show in Fig. 8, all the models are able to reproduce the limit cycle observed in the reference model, but the more accurate seems the TEAM model. To make a quantitative estimation of the accuracy, the Fast Fourier Transform of the time waveform of state variables $x_1(t)$ is reported for each model in Fig. 9. Although the Biolek's

Table 4.
Comparison among the memristor models. For sake of brevity we use the acronym BM to indicate Biolek's Memristor.

	BM	BCM	Team
Test 1	-	✓	-
Test 2-a	✓	✓	✓
Test 2-b	-	-	✓
Test 2-c	✓	✓	-
Test 3	#	#	#

model, the BCM model and the TEAM model present exactly the first harmonic of the reference model (see Fig. 9 and *Test 2-a* in Table 4), it is clear the better accuracy of the TEAM model in capturing higher-order harmonics of the signal referring to the Pickett's model (see Fig. 9 and *Test 2-b* in Table 4). On the other hand, the response to a current pulse of the reference model is reproduced more accurately by the BCM and Biolek's models (see Figs. 10-11 and *Test 2-c* in Table 4).

■ *Result Test 3:* The greater computational complexity in memristor-based nonlinear chaotic circuits may lead to convergence problems and instability issues. The parameters of all memristor models under comparison have been finely tuned in the attempt to reproduce the chaotic attractor observed when the reference model is employed in the circuit of Fig. 12. Extensive numerical simulations have shown that the Biolek's model and the BCM model agree with each other and exhibit chaotic behavior for nearly the same value of the bifurcation parameter as in the case of the Pickett's model (see Sect. IV-B for details). Nonetheless, they are unable to capture the Pickett's model-based chaotic attractor. The TEAM model-based chaotic attractor, observed for a slightly smaller value of the bifurcation parameter (see Sect. IV-B), differs from all the other chaotic attractors. It follows that no memristor model seems to be sufficiently accurate in this case.

All in all, the results are collected in the Table 4 where the symbol ✓ is used to mark the memristor model whose properties result to be qualitatively closer to those of the reference model in the different case-studies. On the other hand, the symbol # is used if no decision can be made.

From the Table 4, we can conclude that the design of novel memristor-based architectures requires the preliminary determination of a universal memristor model.

VI. Outlook on a Novel Model

In this article we discussed the behavior of several memristor models using various excitations and circuits. Our results indicate that simpler models such as Biolek's model and the BCM model seem to be able to reproduce most of the dynamics observed with more accurate models such as the TEAM and the Pickett's models, whose far greater computational complexity may lead to convergence problems and instability issues in the investigation of complex circuits. The parameters of all models greatly depend on the actual circuit under investigation and on its excitation.

As shown in this paper, given a memristor model, a parameter optimization with respect to a reference model may allow one to tune the memristor dynamics so as to reflect the behavior of the reference.

However the parameters of the reference model [16] used throughout the investigations of Section III were fitted to a given circuit and excitation by using data from actual experiments [17]. Parameter sets to arbitrary circuits and excitations are therefore unknown unless one may directly conduct experimental measurements on the physical memristor nano-device.

A simplified and general representation of the dynamics of a memristor is therefore preferable. In the following we present preliminary results of the derivation of a novel model, named Polynomial Model (PM), which takes inspiration from Prof. Chua's idea of unfolding the memristor [5]. As suggested by its name, this model is based upon a polynomial series representation of the state evolution function (let us call it $g(i, w)$, where the arguments show its dependence on state w and input current i). The state equations of the proposed model are expressed as series of polynomials involving w and i :

$$\frac{dw}{dt} = g(i, w) = \sum_{n=0}^N a_n i^n + \sum_{m=0}^M b_m w^m + \sum_{p=1}^P (c_p i + d_p)^p (e_p w + f_p)^p, \quad (33)$$

for $|i| > i_{\min}$ and 0 for $-i_{\min} \leq i \leq i_{\min}$. This novel model attempts to mimic the behavior of Pickett's model by optimizing the series coefficients (i.e. elements of parameter vectors $\mathbf{a} = [a_1, a_2, \dots, a_N]', \mathbf{b} = [b_1, b_2, \dots, b_M]', \mathbf{c} = [c_1, c_2, \dots, c_P]', \mathbf{d} = [d_1, d_2, \dots, d_P]', \mathbf{e} = [e_1, e_2, \dots, e_P]', \mathbf{f} = [f_1, f_2, \dots, f_P]'$) so that equation (33) reproduces the dynamics of the reference model state equations, expressed by (1)-(2).

The first investigations focused on the case of $i < -i_{\min}$, where the variation intervals for current i and state w were chosen so as to match experimental results shown in [16]. Figs. 18 and 19 show the

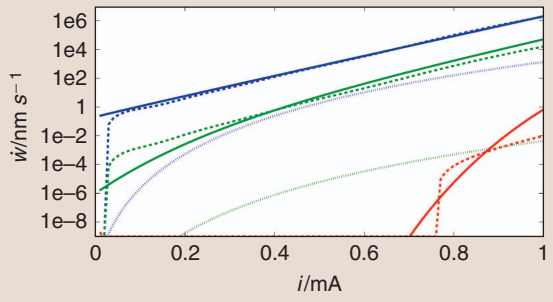


Figure 18. A comparison of the $\dot{w} - i$ characteristics of the Pickett's model, the TEAM model and the PM for a current variation range as suggested by experiments presented in [16]. Pickett's reference model (solid curves), TEAM model (dotted curves) and PM (dashed curves) for $w = 1.1\text{ nm}$ (in blue), $w = 1.475\text{ nm}$ (in green) and $w = 1.85\text{ nm}$ (in red). The units for \dot{w} and i respectively are nm s^{-1} and mA .

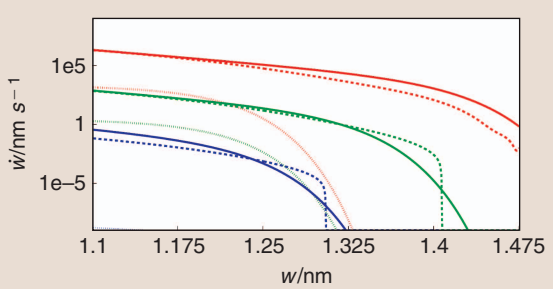


Figure 19. A comparison of the $\dot{w} - w$ characteristics of the Pickett's model, the TEAM model and the PM for a state variation range as suggested by experiments presented in [16]. Pickett's reference model (solid curves), TEAM model (dotted curves) and PM (dashed curves) for $i = 0.06\text{ mA}$ (in blue), $i = 1\text{ mA}$ (in green) and $i = 2\text{ mA}$ (in red). The units for \dot{w} and w respectively are nm s^{-1} and nm .

switching characteristics of the Pickett's model, the TEAM model and the PM with parameters reported in [23]. It should be noted that in this investigation i_{\min} was set to 0.05 mA .

Figs. 18 and 19 reveal the added value a polynomial series expansion of the state evolution function may bring to the current search for a simplified (and at the same time accurate) representation of the Pickett's reference model. In both pictures the PM results outperform the TEAM model predictions.

In these investigations, the parameters given in Tab. 1 were used for the Pickett's model, while the parameters given in column denoted step (1) from Tab. 3 were specified for the TEAM model.

The parameters obtained in our study can be found in Tab. 5. It should be noted that parameter vector $\mathbf{a} = [a_1, a_2, \dots, a_N]'$ was obtained by means of a Taylor series expansion of the reference model for a fixed memristor state w and various values of current i . Here, we

Table 5.
Values of the parameters in the PM state equations (32) for the emulation of the reference model under the simulation scenarios of Figs. 18–19. For sake of brevity the dimensions of the vector coefficients are not reported.

$\mathbf{a} = [a_1, a_2, \dots, a_N]'$			
a_0	a_1	a_2	a_3
0.0111	$-2.300 \cdot 10^3$	$1.24 \cdot 10^8$	$-2.14 \cdot 10^{12}$
a_4	a_5	a_7	a_8
$1.65 \cdot 10^{16}$	$-6.73 \cdot 10^{19}$	$1.60 \cdot 10^{23}$	$-2.27 \cdot 10^{26}$
a_9	a_{10}	a_{11}	
$1.91 \cdot 10^{29}$	$-8.73 \cdot 10^{31}$	$1.68 \cdot 10^{34}$	
$\mathbf{b} = [b_1, b_2, \dots, b_M]'$			
b_0	b_1	b_2	b_3
7.93	-0.2161	-0.2614	-17.9662
b_4	b_5	b_6	b_7
6.77	7.39	1.61	-2.55
b_8	b_9	b_{10}	b_{11}
-2.58	-0.203	2.65	-1.35
b_{12}	b_{13}		
0.202	$7.97 \cdot 10^{-4}$		
$\mathbf{c} = [c_1, c_2, \dots, c_P]'$			
c_1	c_2	c_3	c_4
$5.67 \cdot 10^6$	270.7	-61.9	-7.35
$\mathbf{d} = [d_1, d_2, \dots, d_P]'$			
d_1	d_2	d_3	d_4
$2.48 \cdot 10^8$	1.2868	1.32	-0.53
$\mathbf{e} = [e_1, e_2, \dots, e_P]'$			
e_1	e_2	e_3	e_4
$7.27 \cdot 10^8$	-0.46	-2.53	1.52
$\mathbf{f} = [f_1, f_2, \dots, f_P]'$			
f_1	f_2	f_3	f_4
$1.61 \cdot 10^{12}$	3.92	3.11	1.17

used $N = 11$, $M = 13$ and $P = 4$. The polynomial order of the suggested model is still the subject of ongoing investigations.

An expansion of the model to current values within the closed interval of $-5 \cdot 10^{-5}\text{ A} \leq i \leq 5 \cdot 10^{-5}\text{ A}$ as well as a thorough investigation of its behavior in different circuits and for different excitations shall be the subject of further research. Nevertheless, this represents a first promising step towards a polynomial representation of Pickett's state equations (1) and (2).

This paper sheds some light on the interesting ongoing debate regarding the choice of the most suitable model of memristive nano-structures to be adopted in the investigation of the promising opportunities the memristor offers in integrated circuit design.

VII. Conclusions and Future Research Developments

This paper sheds some light into the interesting ongoing debate regarding the choice of the most suitable model of memristive nano-structures to be adopted in the investigation of the promising opportunities the memristor offers in integrated circuit design, including the emulation of some of the most common learning rules (Hebbian Rule, Spike Timing Dependent Plasticity [27]) at the basis of brain functionalities [31].

In the first part of this work the Pickett's model [16], developed by HP scientists on the basis of laboratory measurements on the TiO_2 -based nano-film, is assumed as the reference to evaluate which of the most noteworthy mathematical models available in literature may be properly optimized so as to capture its dynamics in the case of a scenario for which the parameters of the Pickett model were fitted to the experimental data [17].

The second part of the contribution analyzes the variance of the dynamical behaviors originating in a couple of basic memristor-based circuits according to the memristor model under use. This study is aimed to warn the circuit designers against an indiscriminate use of the memristor models and points out the necessity to develop a universal mathematical model for exploring the full potential of the memristor and unfolding its unique properties [5].

The final part introduces the Polynomial Model (PM), a novel simplified yet accurate version of the Pickett's model. In this model the state evolution function is based upon the series of polynomials involving state and input current. The coefficients of the polynomial series need to be fitted to the Pickett's reference model on the basis of the given circuit and excitation. Preliminary results reveal some improvement in tracking the reference model dynamics in comparison to the TEAM model.



Alon Ascoli received a First Honors Master's Degree in Electronic Engineering from Universita' degli Studi Roma Tre, Rome, Italy, in 2001, and a Ph.D. Degree in Electronic Engineering from University College Dublin, Dublin, Ireland, in 2006. From 2006 to 2009 he enjoyed a fruitful work experience in the Swedish

high-tech industry which allowed him to get extensive expertise in state-of-the-art Analog Integrated Circuit Design and Layout. From 2009 to 2012 he worked as Research Assistant in the Department of Electronics and Telecommunications at Politecnico di Torino, Turin, Italy. Since 2012 he is Researcher and Lecturer in the Faculty of Electrical and Computer Engineering, Technische Universität Dresden, Dresden, Germany. His research interests lie in the area of Nonlinear Circuits and Systems, Networks of Oscillators, Cellular Nonlinear/Neural Networks and Memristive Systems including their applications. Dr. Ascoli was honored with the International Journal of Circuit Theory and Its Applications 2007 Best Paper Award for his publication entitled "Modelling the dynamics of log-domain circuits". He serves as Reviewer for various Peer-Reviewed Journal Papers including the *International Journal of Circuit Theory and Its Applications* and the *IEEE Transactions on Circuits and Systems-I*. He currently teaches a graduate course on Cellular Neural Networks.



Fernando Corinto (M'03–SM'10) received the Laurea degree in Electronics and the Ph.D. degree in Electronics and Communications Engineering in 2001 and in 2005, respectively, and the European Doctorate in 2005, all from the Politecnico di Torino, Torino, Italy.

In 2004, he won a Marie Curie Fellowship (within the Marie Curie Actions under the Sixth Framework Programme). He is currently an Assistant Professor of Circuit Theory with the Dipartimento di Elettronica, Politecnico di Torino. His research activities are mainly in the areas of nonlinear circuits and systems, locally coupled nonlinear/nanoscale networks and memristor technology. He is coauthor of more than 90 international journal and conference papers. He has been reviewer of several papers for international journals and conferences and chair of sessions in international conferences. He is the principal investigator of several research projects. Since 2010, he is Senior Member of the IEEE, Member of the IEEE CAS Technical Committees on: Cellular Nanoscale Networks and Array Computing and Nonlinear Circuit and Systems. Fernando Corinto was the Technical Program Chair for the 13th Workshop on Cellular Nanoscale Networks and their Applications and 3rd

Symposium on Memristor. He is also Visiting Professor at PPCU of Budapest, since 2007.



Vanessa Senger received her Diploma of Physics Degree in 2009 from the Goethe University in Frankfurt and is currently doing her PhD in electrical engineering at the Technical University of Dresden. Her research interests include Cellular Nonlinear Networks, Memristive Systems and Nonlinear Signal Processing.



Ronald Tetzlaff is a Full Professor of Fundamentals of Electrical Engineering at the Technische Universität Dresden, Germany. His scientific interests include problems in the theory of signals and systems, stochastic processes, physical fluctuation phenomena, system modeling, system identification, Volterra systems, Cellular Nonlinear Networks, and Memristive Systems. From 1999 to 2003 Ronald Tetzlaff was Associate Editor of the *IEEE Transactions on Circuits and Systems: Part I*. He was “Distinguished Lecturer” of the IEEE CAS Society (2001-2002). He is a member of the scientific committee of different international conferences. He was the chair of the 7th IEEE International Workshop on Cellular Neural Networks and their Applications (CNNA 2002), of the 18th IEEE Workshop on Nonlinear Dynamics of Electronic Systems (NDES 2010) and of the 5th International Workshop on Seizure Prediction (IWSP 2011). Ronald Tetzlaff is in the Editorial Board of the *International Journal of Circuit Theory and Applications* since 2007 and he is also in the Editorial Board of the *AEÜ—International Journal of Electronics and Communications* since 2008. He serves as a reviewer for several journals and for the European Commission. From 2005 to 2007 he was the chair of the IEEE Technical Committee Cellular Neural Networks & Array Computing. He is a member of the Informationstechnische Gesellschaft (ITG) and the German Society of Electrical Engineers and of the German URSI Committee.

References

- [1] L. O. Chua, “Memristor: The missing circuit element,” *IEEE Trans. Circuit Theory*, vol. 18, no. 5, pp. 507–519, 1971.
- [2] L. O. Chua, “The fourth element,” *Proc. IEEE*, vol. 100, no. 6, pp. 1920–1927, 2012.
- [3] D. Biolek, Z. Biolek, V. Biolková, and Z. Kolka, “Some fingerprints of ideal memristors,” in *Proc. Int. Symp. Circuits and Systems*, 2013.
- [4] F. Corinto, A. Ascoli, and M. Gilli, “Analysis of current–voltage characteristics for memristive elements in pattern recognition systems,” *Int. J. Circuit Theory Appl.*, 2012, doi: 10.1002/cta.1804.
- [5] L. O. Chua, “Resistance switching memories are memristors,” *Appl. Phys. A*, vol. 102, no. 4, pp. 765–783, 2011.
- [6] L. O. Chua and S. M. Kang, “Memristive devices and systems,” *Proc. IEEE*, vol. 64, no. 2, pp. 209–223, 1976.
- [7] F. Corinto and A. Ascoli, “Memristive diode bridge with LCR filter,” *Electron. Lett.*, vol. 14, pp. 824–825, 2012.
- [8] D. B. Strukov, G. S. Snider, D. R. Stewart, and R. S. Williams, “The missing memristor found,” *Nature*, vol. 453, pp. 80–83, 2008.
- [9] A. C. Torrezan, J. P. Strachan, G. Medeiros-Ribeiro, and R. S. Williams, “Sub-nanosecond switching of a tantalum oxide memristor,” *Nanotechnology*, vol. 22, no. 48, pp. 485203(1)–485203(7), 2011, doi: 10.1088/0957-4484/22/48/485203.
- [10] F. Corinto, A. Ascoli, and M. Gilli, “Nonlinear dynamics of memristor oscillators,” *IEEE Trans. Circuits Syst. I, Reg. Papers*, vol. 58, no. 6, pp. 1323–1336, June 2011.
- [11] A. Talukdar, A. G. Radwan, and K. N. Salama, “Nonlinear dynamics of memristor based 3rd order oscillatory system,” *Microelectron. J.*, vol. 43, no. 3, pp. 169–175, 2012.
- [12] D. B. Strukov, D. R. Stewart, J. L. Borghetti, X. Li, M. Pickett, G. M. Ribeiro, W. Robinett, G. S. Snider, J. P. Strachan, W. Wu, Q. Xia, J. J. Yang, and R. S. Williams, “Hybrid CMOS/memristor circuits,” *Proc. Int. Symp. Circuits and Systems*, 2010, pp. 1967–1970.
- [13] M. Versace and B. Chandler, “MoNETA: A mind made from memristors,” *IEEE Spectr.*, Dec. 2010.
- [14] Y. V. Pershin, S. La Fontaine, and M. Di Ventra, “Memristive model of amoeba learning,” *Phys. Rev. E*, vol. 80, no. 2, pp. 021926(1)–021926(6), 2009.
- [15] G. K. Johnsen, “An introduction to the memristor: A valuable circuit element in bioelectricity and bioimpedance,” *J. Electr. Bioimp.*, vol. 3, pp. 20–28, 2012.
- [16] M. D. Pickett, D. B. Strukov, J. L. Borghetti, J. J. Yang, G. S. Snider, D. R. Stewart, and R. S. Williams, “Switching dynamics in titanium dioxide memristive devices,” *J. Appl. Phys.*, vol. 106, p. 074508, 2009.
- [17] H. Abdalla and M. D. Pickett, “SPICE modeling of memristors,” in *Proc. IEEE Int. Symp. Circuits and Systems*, May 2011, pp. 1832–1835.
- [18] Y. N. Joglekar and S. T. Wolf, “The elusive memristor: Properties of basic electrical circuits,” *Eur. J. Phys.*, vol. 30, pp. 661–675, 2009.
- [19] Z. Biolek, D. Biolek, and B. Biolková, “Spice model of memristor with nonlinear dopant drift,” *Radio Eng.*, vol. 18, no. 2, pp. 210–214, 2009.
- [20] T. Prodromakis, B. P. Peh, C. Papavassiliou, and C. Toumazou, “A versatile memristor model with non-linear dopant kinetics,” *IEEE Trans. Electron Devices*, vol. 58, no. 9, 2011.
- [21] A. Rak and G. Cserey, “Macromodeling of the memristor in SPICE,” *IEEE Trans. Comput.-Aided Design Integr. Circuits Syst.*, vol. 29, no. 4, pp. 632–636, Apr. 2010.
- [22] F. Corinto and A. Ascoli, “A boundary condition-based approach to the modeling of memristor nanostructures,” *IEEE Trans. Circuits Syst. I, Reg. Papers*, vol. 59, no. 11, pp. 2713–2726, Nov. 2012, doi: 10.1109/TCSI.2012.2190563.
- [23] S. Kvatsinsky, E. G. Friedman, A. Kolodny, and U. C. Weiser, “TEAM: ThrEshold Adaptive Memristor model,” *IEEE Trans. Circuits Syst. I, Reg. Papers*, vol. 60, no. 1, pp. 211–221, 2013.
- [24] S. P. Brooks and B. J. T. Morgan, “Optimization using simulated annealing,” *J. Roy. Stat. Soc. D (Statist.)*, vol. 44, no. 2, pp. 241–257, 1995.
- [25] J. A. Snyman, *Practical Mathematical Optimization: An Introduction to Basic Optimization Theory and Classical and New Gradient-Based Algorithms*. Springer, 2005, 278 pp.
- [26] J. Simmons, “Electric tunnel effect between dissimilar electrodes separated by a thin insulating film,” *J. Appl. Phys.*, vol. 34, no. 9, pp. 2581–2590, 1963.
- [27] A. Ascoli, R. Tetzlaff, and F. Corinto, “Generalized memristor boundary condition model and its PSpice circuit,” *IEEE Trans. Circuits Systems I, Reg. Papers*, submitted for publication.
- [28] K. Eshraghian, O. Kavehei, K.-R. Cho, J. M. Chappell, A. Iqbal, S. F. Al-Sarawi, and D. Abbott, “Memristive device fundamentals and modeling: Applications to circuits and systems simulation,” *Proc. IEEE*, vol. 100, no. 6, pp. 1991–2007, June 2012, doi: 10.1109/JPROC.2012.2188770.
- [29] A. Ascoli, R. Tetzlaff, F. Corinto, and M. Gilli, “PSpice switch-based versatile memristor model,” in *Proc. Int. Symp. Circuits and Systems*, Beijing, May 2013.
- [30] M. Itoh and L. Chua, “Memristor oscillators,” *Int. J. Bifurcat. Chaos*, vol. 18, no. 11, pp. 3183–3206, 2008.
- [31] R. S. Williams, “How we found the missing memristor,” *IEEE Spectr.*, pp. 29–35, Dec. 2008.